# Mesoscale Modeling of Hydrated Morphologies of 3M Perfluorosulfonic Acid–Based Fuel Cell Electrolytes

**ARTICLE** *in* LANGMUIR · SEPTEMBER 2010

Impact Factor: 4.46 · DOI: 10.1021/la102358y · Source: PubMed



**4 AUTHORS**, INCLUDING:

Stephen J Paddison
University of Tennessee
**128** PUBLICATIONS **3,951** CITATIONS

SEE PROFILE

James A Elliott
University of Cambridge
**127** PUBLICATIONS **2,782** CITATIONS

SEE PROFILE

Langmuir
Article
pubs.acs.org/Langmuir


# Mesoscale Modeling of Hydrated Morphologies of 3M Perfluorosulfonic Acid-Based Fuel Cell Electrolytes

Dongsheng Wu,[†] Stephen J. Paddison,*[,†] James A. Elliott,[‡] and Steven J. Hamrock[§]

[†]*Department of Chemical and Biomolecular Engineering, University of Tennessee, Knoxville, Tennessee 37996,* [‡]*Department of Materials Science and Metallurgy, University of Cambridge, Pembroke Street, Cambridge CB2 3QZ, U.K., and* [§]*3M Fuel Cell Components Program, 3M Center, St. Paul, Minnesota 55144*

*Received June 9, 2010. Revised Manuscript Received July 29, 2010*

Dissipative particle dynamics (DPD) simulations have been carried out to study the hydrated morphology of 3M perfluorosulfonic acid (PFSA) fuel cell membranes as a function of the equivalent weight (EW), molecular weight (MW), and hydration level. The 3M PFSA ionomers were modeled using typical EWs of 578, 640, and 790 g/mol, and molecular weights were varied from about 45 000 to 90 000 g/mol in order to be close to the experimental range. The morphology changes corresponding to the EW, MW, and hydration level were comparatively investigated by inspecting the water distributions, followed by quantitative analysis by radial distribution functions and Bragg spacing according to the periodicity of water domains. Compared to the morphologies of short-side-chain PFSA membrane (Wu, D.; Paddison, S. J.; Elliott, J. A. *Macromolecules* **2009**, *42*, 3358−3367), the longer side chain in 3M PFSA membrane provides more flexibility for the sulfonate-terminated side chains and generally results in the stronger aggregation of water clusters. This results in lower water uptake for higher EW, corresponding to a lower ion-exchange capacity (IEC), which is attributed experimentally to a higher crystallinity of the fluorocarbon phase, although our simulations were not able to observe the crystallites directly.

## Introduction

Proton-exchange membrane fuel cells (PEMFCs) have been widely developed and explored in the last four decades. Although not without some problematic issues, such as durability, cost, and availability of raw materials, they are still considered to be the most promising alternative power source for vehicles, portable devices, and some stationary applications. To achieve these ends, tremendous research effort has been devoted to the development and characterization of novel electrolyte materials in order to overcome the remaining drawbacks (e.g., operating temperature and humidification requirements) of the present polymer electrolytes.[1−4]

Among various chemistries developed for electrolyte membranes, perfluorosulfonic acid (PFSA) membranes remain the most commonly employed because of their chemical stability and high selectivity. Nafion in particular remains the benchmark standard for PFSA membranes because of its long history of use and comprehensive characterization as a membrane material.[5] However, the limitations of Nafion, such as its restrictive range of thermal stability and the requirement of a significant level of hydration, have driven the development of Flemion, Aciplex, the short-side-chain (SSC) membrane[6−12] (originally synthesized by Dow Chemical and now manufactured by Solvay Solexis as Aquivion),[13−17] and the 3M membrane.[2,18,19] Compared to the short side chain in the Dow membrane, the 3M PFSA membrane has a slightly longer $-O(CF_2)_4SO_3H$ side chain, although there is no secondary ether linkage as in the Nafion side chain. The 3M PFSA membranes with

*To whom correspondence should be addressed. E-mail: spaddison@utk.edu.

(1) Yoshitake, M.; Watakabe, A. Perfluorinated Ionic Polymers for PEFCs (Including Supported PFSA). In *Fuel Cells 1*; Scherer, G. G., Ed.; Advances in Polymer Science 215; Springer: New York, 2008; pp 127−155.

(2) Hamrock, S. J.; Yandrasits, M. A. Proton exchange membranes for fuel cell applications. *Polym. Rev.* **2006**, *46*, 219−244.

(3) Lee, J. S.; Quan, N. D.; Hwang, J. M.; Lee, S. D.; Kim, H.; Lee, H.; Kim, H. S. Polymer electrolyte membranes for fuel cells. *J. Ind. Eng. Chem.* **2006**, *12*, 175−183.

(4) Paddison, S. J. Proton conduction mechanisms at low degrees of hydration in sulfonic acid-based polymer electrolyte membranes. *Annu. Rev. Mater. Res.* **2003**, *33*, 289−319.

(5) Mauritz, K. A.; Moore, R. B. State of understanding of Nafion. *Chem. Rev.* **2004**, *104*, 4535−4585.

(6) Tant, M. R.; Lee, K. D.; Darst, K. P.; Martin, C. W. Effect of side-chain length on the properties of perfluorocarbon ionomers. *Polym. Mater. Sci. Eng.* **1988**, *58*, 1074.

(7) Moore, R. B.; Martin, C. R. Morphology and chemical properties of the Dow perfluorinated ionomers. *Macromolecules* **1989**, *22*, 3594−3599.

(8) Eisman, G. A. The application of Dow Chemical's perfluorinated membranes in proton-exchange membrane fuel cells. *J. Power Sources* **1990**, *29*, 389−398.

(9) Gebel, G.; Moore, R. B. Small-angle scattering study of short pendant chain perfluorosulfonated ionomer membranes. *Macromolecules* **2000**, *33*, 4850−4855.

(10) Ghielmi, A.; Vaccarono, P.; Troglia, C.; Arcella, V. Proton exchange membranes based on the short-side-chain perfluorinated ionomer. *J. Power Sources* **2005**, *145*, 108−115.

(11) Kreuer, K. D.; Schuster, M.; Obliers, B.; Diat, O.; Traub, U.; Fuchs, A.; Klock, U.; Paddison, S. J.; Maier, J. Short-side-chain proton conducting perfluorosulfonic acid ionomers: why they perform better in PEM fuel cells. *J. Power Sources* **2008**, *178*, 499−509.

(12) Gorri, D.; De Angelis, M. G.; Giacinti Baschetti, M.; Sarti, G. C. Water and methanol permeation through short-side-chain perfluorosulphonic acid ionomeric membranes. *J. Membr. Sci.* **2008**, *322*, 383−391.

(13) Arcella, V.; Ghielmi, A.; Tommasi, G. High performance perfluoropolymer films and membranes. *Ann. N.Y. Acad. Sci.* **2003**, *984*, 226−244.

(14) Arcella, V.; Troglia, C.; Ghielmi, A. Hyflon ion membranes for fuel cells. *Ind. Eng. Chem. Res.* **2005**, *44*, 7646−7651.

(15) Merlo, L.; Ghielmi, A.; Cirillo, L.; Gebert, M.; Arcella, V. Resistance to peroxide degradation of Hyflon® ion membranes. *J. Power Sources* **2007**, *171*, 140−147.

(16) Merlo, L.; Ghielmi, A.; Cirillo, L.; Gebert, M.; Arcella, V. Membrane electrode assemblies based on HYFLON (R) ion for an evolving fuel cell technology. *Sep. Sci. Technol.* **2007**, *42*, 2891−2908.

(17) Navarrini, W.; Scrosati, B.; Panero, S.; Ghielmi, A.; Sanguineti, A.; Geniram, G. Lithiated short side chain perfluorinated sulfonic ionomeric membranes: water content and conductivity. *J. Power Sources* **2008**, *178*, 783−788.

(18) Haugen, G. M.; Meng, F. Q.; Aieta, N. V.; Horan, J. L.; Kuo, M. C.; Frey, M. H.; Hamrock, S. J.; Herring, A. M. The effect of heteropoly acids on stability of PFSA PEMs under fuel cell operation. *Electrochem. Solid State Lett.* **2007**, *10*, B51−B55.

(19) Aieta, N. V.; Stanis, R. J.; Horan, J. L.; Yandrasits, M. A.; Cookson, D. J.; Ingham, B.; Toney, M. F.; Hamrock, S. J.; Herring, A. M. Clipped random wave morphologies and the analysis of the SAXS of an ionomer formed by copolymerization of tetrafluoroethylene and $CF_2{=}CFO(CF_2)_4SO_3H$. *Macromolecules* **2009**, *42*, 5774−5780.

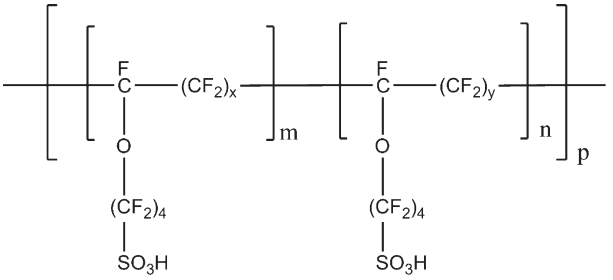

**Figure 1.** General structure of the macromolecules of the 3M PFSA ionomer used in the DPD simulations. Distinct $x$ and $y$ values give different backbone lengths, the selection of $m$ and $n$ determine the average EW, and the value of $p$ determines the MW of the ionomer.

low equivalent weights (EWs) have been observed to exhibit high proton conductivities and good thermal stability and mechanical properties when compared to Nafion 1100.[2] However, the morphology of 3M PFSA membranes has not been as comprehensively examined.

Recently, Aieta et al. carried out small-angle X-ray scattering (SAXS) on 3M PFSA membranes of various EWs.[19] Combining a unified fit approach and the clipped random wave morphology (CRW) method, they generated very similar morphologies to those obtained in our previous dissipative particle dynamics (DPD) simulations of PFSA membranes,[20,21] consisting of a bicontinuous phase of hydrophilic and hydrophobic regions. Such morphologies are also consistent with earlier attempts to produce a model-independent fit to the SAXS data for Nafion using maximum entropy techniques.[22,23] Furthermore, Haugen et al. added various heteropoly acids (HPAs) to operating fuel cells assembled with 3M membranes and found out that the stable HPAs led to longer lifetimes and improved performance.[18] However, to obtain an improved understanding of how morphology is connected with membrane properties, a multiscale computational approach is required.

Over the past decade, multiscale modeling and simulation have been carried out to provide a better understanding of the structure, morphology, and functionality of PFSA membranes.[24] Because of the large size of the systems under study, various modeling techniques must be applied at different size scales because no single method is able to span the entire range. The structural correlations and transport properties of PFSAs have been studied with classical molecular dynamics (MD) simulations,[25] together with empirical valence bond (EVB) models of the solvation and transport of hydrated protons.[26−28] Coarse-grained MD simulations have also been used to study the effect of water on the phase-segregated morphology of the Nafion ionomer.[29] Mesoscale modeling involving DPD simulation was first carried out by Yamamoto and Hyodo to investigate the mesoscopic structure of Nafion at various degrees of hydration.[30] The present authors have also implemented DPD simulation to comparatively study the different morphologies in Nafion, short-side-chain (SSC), and 3M membranes as a function of the side chain length, together with the effect of molecular and equivalent weights on the morphological changes.[20,21] Self-consistent mean field (SCMF) simulations have also been employed to study the morphological changes in Nafion with respect to temperature and water content.[31] These differ in their approach from DPD in that rather than solving explicitly for the positions of the mesoscopic particles, their density distributions are evolved under the influence of a slowly varying external potential in which the free energy of the system is minimized. Wescott et al. used the MESODYN code, which is based on such a mean-field free-energy functional approach, to study the morphology of hydrated PFSA membranes analogous to Nafion 117.[32] They also found phase-separated morphologies in all cases, but percolation of the water-rich phase was found only for water contents higher than those required experimentally for conductivity. It is thus clear that structures on a smaller scale than ionic clusters also play an important role in achieving protonic conductivity.

In the present work, we have studied the morphology of the 3M PFSA membrane by systematically investigating the effect of the equivalent weight (EW), molecular weight (MW), and water content. The EWs were modeled at three different values of 578, 640, and 790 g/mol, and the MWs were varied in the range from about 45 000 to 90 000 g/mol. The values of the EWs were chosen so as to be a close match to experimental data for typical 3M membranes. Although there is limited specific information

**Table 1. Macromolecule Parameters for the Selected EWs and MWs**

| EW | MW | $x$ | $y$ | $m$ | $n$ | $p$ |
|---|---|---|---|---|---|---|
| 578 | 45 084 | 1 | 7 | 1 | 2 | 26 |
| | 90 168 | 1 | 7 | 1 | 2 | 52 |
| 640 | 46 116 | 1 | 7 | 1 | 7 | 9 |
| | 92 232 | 1 | 7 | 1 | 7 | 18 |
| 790 | 44 268 | 7 | 13 | 5 | 3 | 7 |
| | 88 536 | 7 | 13 | 5 | 3 | 14 |

**Table 2. Computed $\chi$ Parameters and Corresponding Repulsion Parameters Describing Pairwise Conservative Interactions of Selected Beads for the 3M PFSA Ionomer**

| pair[a] | $\chi$ | $a_{ij}$ ($k_BT$) |
|---|---|---|
| A−B | −0.03 | 24.9 |
| A−C | 7.07 | 48.1 |
| A−W | 3.30 | 35.8 |
| B−C | 7.04 | 48.0 |
| B−W | 3.47 | 36.3 |
| C−W | 1.53 | 30.0 |

[a] DPD beads in pairs are (A) $-CF_2CF_2CF_2CF_2CF_2CF_2-$, (B) $-CF_2CF(OCF_2CF_2CF_2)-$, (C) $-CF_2SO_3H\cdot 3H_2O$, and (W) $6H_2O$.

(20) Wu, D.-S.; Paddison, S. J.; Elliott, J. A. A comparative study of the hydrated morphologies of perfluorosulfonic acid fuel cell membranes with mesoscopic simulations. *Energy Environ. Sci.* **2008**, *1*, 284−293.
(21) Wu, D. S.; Paddison, S. J.; Elliott, J. A. Effect of molecular weight on hydrated morphologies of the short-side-chain perfluorosulfonic acid membrane. *Macromolecules* **2009**, *42*, 3358−3367.
(22) Elliott, J. A.; Hanna, S. A model-independent maximum-entropy method for the inversion of small-angle X-ray diffraction patterns. *J. Appl. Crystallogr.* **1999**, *32*, 1069−1083.
(23) Elliott, J. A.; Hanna, S.; Elliott, A. M. S.; Cooley, G. E. Interpretation of the small-angle X-ray scattering from swollen and oriented perfluorinated ionomer membranes. *Macromolecules* **2000**, *33*, 4161−4171.
(24) Elliott, J. A.; Paddison, S. J. Modelling of morphology and proton transport in PFSA membranes. *Phys. Chem. Chem. Phys.* **2007**, *9*, 2602−2618.
(25) Hristov, I. H.; Paddison, S. J.; Paul, R. Molecular modeling of proton transport in the short-side-chain perfluorosulfonic acid ionomer. *J. Phys. Chem. B* **2008**, *112*, 2937−2949.
(26) Blake, N. P.; Mills, G.; Metiu, H. Dynamics of $H_2O$ and $Na^+$ in Nafion membranes. *J. Phys. Chem. B* **2007**, *111*, 2490−2494.
(27) Blake, N. P.; Petersen, M. K.; Voth, G. A.; Metiu, H. Structure of hydrated Na−Nafion polymer membranes. *J. Phys. Chem. B* **2005**, *109*, 24244−24253.
(28) Petersen, M. K.; Wang, F.; Blake, N. P.; Metiu, H.; Voth, G. A. Excess proton solvation and delocalization in a hydrophilic pocket of the proton conducting polymer membrane Nafion. *J. Phys. Chem. B* **2005**, *109*, 3727−3730.
(29) Malek, K.; Eikerling, M.; Wang, Q. P.; Liu, Z. S.; Otsuka, S.; Akizuki, K.; Abe, M. Nanophase segregation and water dynamics in hydrated Nafion: molecular modeling and experimental validation. *J. Chem. Phys.* **2008**, *129*, 204702.
(30) Yamamoto, S.; Hyodo, S. A. A computer simulation study of the mesoscopic structure of the polyelectrolyte membrane Nafion. *Polym. J.* **2003**, *35*, 519−527.
(31) Galperin, D. Y.; Khokhlov, A. R. Mesoscopic morphology of proton-conducting polyelectrolyte membranes of Nafion® type: a self-consistent mean field simulation. *Macromol. Theory Simul.* **2006**, *15*, 137−146.
(32) Wescott, J. T.; Qi, Y.; Subramanian, L.; Capehart, T. W. Mesoscale simulation of morphology in hydrated perfluorosulfonic acid membranes. *J. Chem. Phys.* **2006**, *124*, 134702.

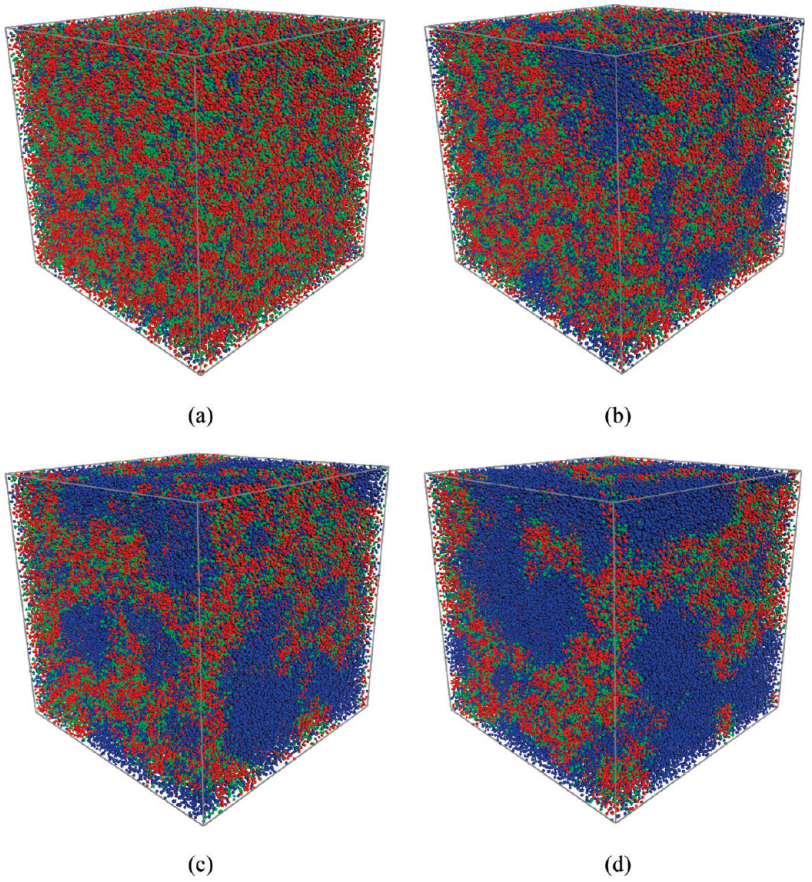


**Figure 2.** Hydrated morphologies of the 3M PFSA ionomer with EW = 640 and MW = 46 116 g/mol at water contents of (a) $\lambda = 6$, (b) $\lambda = 12$, (c) $\lambda = 18$, and (d) $\lambda = 24$ $H_2O/SO_3H$. Fluorocarbon backbone and side-chain beads of type A and B are red, hydrated side-chain beads of type C are green, and water beads of type W are blue.

about the MW for the 3M polymer, a range of between $10^5$ and $10^6$ g/mol is generally accepted for PFSAs.[33] GPC analysis indicates that the 3M ionomer falls in this range.[34] Water contents of 6, 12, 18, and 24 $H_2O/SO_3H$ were selected because these encompass the full range of hydration observed in the membrane of operating fuel cells. The 3M PFSA membranes were then modeled by connecting soft spherical beads (DPD particles), and Flory−Huggins $\chi$ parameters were calculated for each coarse-grained particle to derive the corresponding interaction parameters for the DPD simulations. On the basis of DPD calculated densities, the radial distribution functions (RDFs) for water particles were generated to characterize the water clusters. Finally, the average Bragg spacing between water clusters was calculated from the scattering intensities according to the Fourier-transformed RDFs.

## Modeling and Calculations

**DPD Simulations and Modeling for 3M PFSA Membranes.** The DPD method has been well established since its first introduction by Hoogerbrugge and Koelman to simulate the complex hydrodynamic behavior of isothermal fluids[35,36] and further development by Español to include stochastic differential equations and the conservation of energy.[37,38] The interaction between two DPD particles is expressed as the sum of the conservative force $\mathbf{F}_{ij}^{C}$, dissipative force $\mathbf{F}_{ij}^{D}$, random force $\mathbf{F}_{ij}^{R}$, and harmonic spring force $\mathbf{F}_{ij}^{S}$ for the system:

$$\mathbf{f}_i = \sum_{j \neq i} (\mathbf{F}_{ij}^{C} + \mathbf{F}_{ij}^{D} + \mathbf{F}_{ij}^{R} + \mathbf{F}_{ij}^{S}) \quad (1)$$

The conservative force is derived from a potential exerted on particle $i$ by the $j$th particle[39] and treated as a soft repulsion action along the line of centers with the form[40,41]

$$\mathbf{F}_{ij}^{C} = \begin{cases} a_{ij}(r_c - r_{ij})\mathbf{n}_{ij} & r_{ij} < r_c \\ 0 & r_{ij} \geq r_c \end{cases} \quad (2)$$

where $a_{ij}$ is a maximum repulsion force between particles $i$ and $j$, $r_c$ is a selected cutoff radius of the interaction, $\mathbf{r}_{ij} = \mathbf{r}_i - \mathbf{r}_j$, $r_{ij} = |\mathbf{r}_{ij}|$, and $\mathbf{n}_{ij} = \mathbf{r}_{ij}/|\mathbf{r}_{ij}|$. The repulsive interaction parameters $a_{ij}$ required

(33) Curtin, D. E.; Lousenberg, R. D.; Henry, T. J.; Tangeman, P. C.; Tisack, M. E. Advanced materials for improved PEMFC performance and life. *J. Power Sources* **2004**, *131*, 41−48.
(34) Hamrock, S. J. Unpublished results.
(35) Hoogerbrugge, P. J.; Koelman, J. M. V. A. Simulating microscopic hydrodynamic phenomena with dissipative particle dynamics. *Europhys. Lett.* **1992**, *19*, 155−160.
(36) Koelman, J. M. V. A.; Hoogerbrugge, P. J. Dynamic simulations of hard-sphere suspensions under steady shear. *Europhys. Lett.* **1993**, *21*, 363−368.
(37) Español, P.; Warren, P. B. Statistical mechanics of dissipative particle dynamics. *Europhys. Lett.* **1995**, *30*, 191−196.
(38) Español, P. Dissipative particle dynamics with energy conservation. *Europhys. Lett.* **1997**, *40*, 631−636.
(39) Groot, R. D.; Warren, P. B. Dissipative particle dynamics: bridging the gap between atomistic and mesoscopic simulation. *J. Chem. Phys.* **1997**, *107*, 4423−4435.
(40) Groot, R. D.; Madden, T. J. Dynamic simulation of diblock copolymer microphase separation. *J. Chem. Phys.* **1998**, *108*, 8713−8724.
(41) Groot, R. D.; Rabone, K. L. Mesoscopic simulation of cell membrane damage, morphology change and rupture by nonionic surfactants. *Biophys. J.* **2001**, *81*, 725−736.

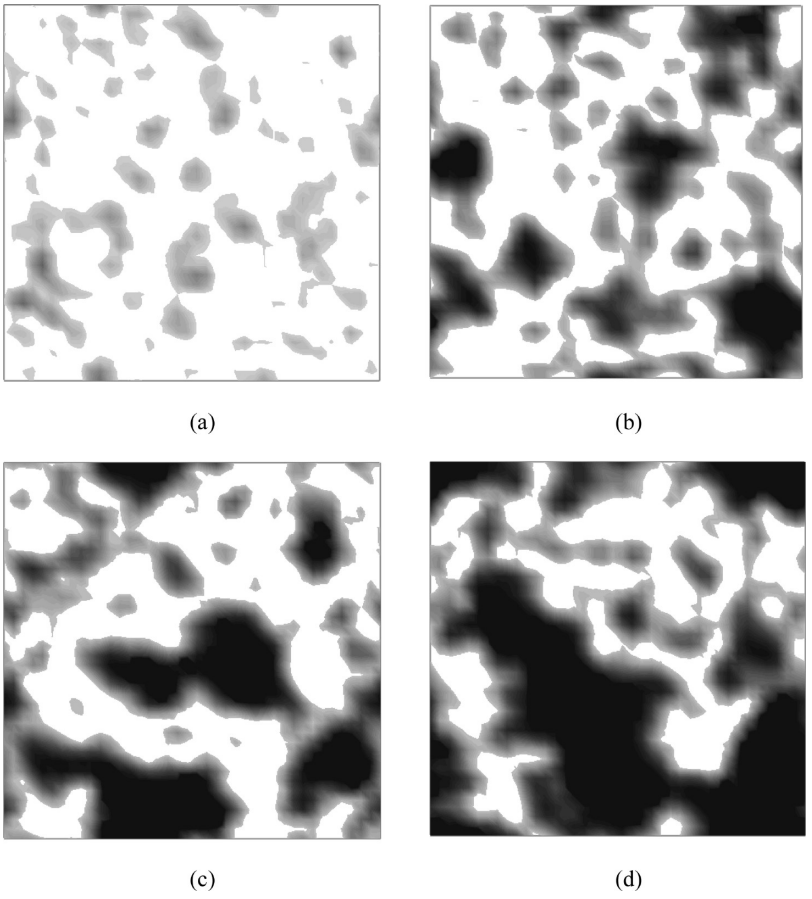


**Figure 3.** Contour plots of the density of the water beads as a 2D cross section of the hydrated morphologies with EW = 640 and MW = 46 116 g/mol (shown in Figure 2) at water contents of (a) $\lambda = 6$, (b) $\lambda = 12$, (c) 18, and (d) $\lambda = 24$ $H_2O/SO_3H$. The darkness of the gray level is linearly proportional to the water density (i.e., darker regions correspond to water-rich areas).

for the calculation of conservative forces are related to the Flory−Huggins $\chi$ parameter as follows[39,40]

$$a_{ij} = a_{ii} + 3.27\chi \quad (3)$$

where $a_{ii}$ is the repulsion parameter between particles of the same type and has a value of $25k_BT$. The dissipative force, random force, and spring force correspond to the viscous drag, thermal motion, and a harmonic potential, respectively. With all interactions defined, the positions and velocities of the DPD particles can be solved by implementing Newton's equation of motion and a modified version of the velocity Verlet algorithm.[39]

The general molecular structure for the simulated 3M PFSA ionomers is shown in Figure 1. The values of $x$ and $y$ determine the EWs of two corresponding monomers. By varying the $m$ and $n$ values, the average EWs between those of the two monomers can be generated. Hence, values for these parameters were selected to given EWs of 578, 640, and 790 g/mol and are summarized in Table 1. With the further selection of specific values for $p$ (Table 1), we constructed MWs of 45 084 and 90 168 g/mol for EW = 578, MWs of 46 116 and 92 232 g/mol for EW = 640, and MWs of 44 268 and 88 536 g/mol for EW = 790. The polymer is modeled by connecting spherical soft particles (beads) that contain groups of atoms and/or molecules. The ionomer consists of three distinct DPD beads in the present simulations, denoted A, B, and C, which correspond to $-CF_2CF_2CF_2CF_2CF_2CF_2-$, $-CF_2CF(OCF_2CF_2CF_2)-$, and $-CF_2SO_3H\cdot 3H_2O$, respectively. Another independent water particle, denoted W, was constructed from six water molecules. The choice of the structure of the beads was based on the requirement for similar sizes of different beads and the flexibility of generating different EWs and hydration levels for the systems. The structures of particles A, B, and W were optimized using molecular mechanics with COMPASS parameters using the Forcite module in the Materials Studio software package.[42] The structure of particle C was optimized using the B3LYP hybrid density functional and the 6-31G** basis set as implemented in Gaussian 03.[43] This treatment of the C bead was deemed necessary because of the observed dissociation of the proton from the sulfonic acid groups at water contents of $\geq 3$ $H_2O/SO_3H$.[44,45] The Flory−Huggins $\chi$ parameters were calculated at room temperature with COMPASS force field

(42) *Materials Studio*, version 4.1; Accelrys Software Inc.: San Diego, CA, 2006.
(43) Frisch, M. J.; Trucks, G. W.; Schlegel, H. B.; Scuseria, G. E.; Robb, M. A.; Cheeseman, J. R.; Montgomery, J. A.; Vreven, T.; Kudin, K. N.; Burant, J. C.; Millam, J. M.; Iyengar, S. S.; Tomasi, J.; Barone, V.; Mennucci, B.; Cossi, M.; Scalmani, G.; Rega, N.; Petersson, G. A.; Nakatsuji, H.; Hada, M.; Ehara, M.; Toyota, K.; Fukuda, R.; Hasegawa, J.; Ishida, M.; Nakajima, T.; Honda, Y.; Kitao, O.; Nakai, H.; Klene, M.; Li, X.; Knox, J. E.; Hratchian, H. P.; Cross, J. B.; Adamo, C.; Jaramillo, J.; Gomperts, R.; Stratmann, R. E.; Yazyev, O.; Austin, A. J.; Cammi, R.; Pomelli, C.; Ochterski, J. W.; Ayala, P. Y.; Morokuma, K.; Voth, G. A.; Salvador, P.; Dannenberg, J. J.; Zakrzewski, V. G.; Dapprich, S.; Daniels, A. D.; Strain, M. C.; Farkas, O.; Malick, D. K.; Rabuck, A. D.; Raghavachari, K.; Foresman, J. B.; Ortiz, J. V.; Cui, Q.; Baboul, A. G.; Clifford, S.; Cioslowski, J.; Stefanov, B. B.; Liu, G.; Liashenko, A.; Piskorz, P.; Komaromi, I.; Martin, R. L.; Fox, D. J.; Keith, T.; Al-Laham, M. A.; Peng, C. Y.; Nanayakkara, A.; Challacombe, M.; Gill, P. M. W.; Johnson, B.; Chen, W.; Wong, M. W.; Gonzalez, C.; Pople, J. A. *Gaussian 03*, Revision C.02; Gaussian Inc.: Wallingford, CT, 2004.
(44) Paddison, S. J. The modeling of molecular structure and ion transport in sulfonic acid based ionomer membranes. *J. New Mater. Electrochem. Syst.* **2001**, *4*, 197−207.
(45) Paddison, S. J.; Elliott, J. A. On the consequences of side chain flexibility and backbone conformation on hydration and proton dissociation in perfluorosulfonic acid membranes. *Phys. Chem. Chem. Phys.* **2006**, *8*, 2193−2203.

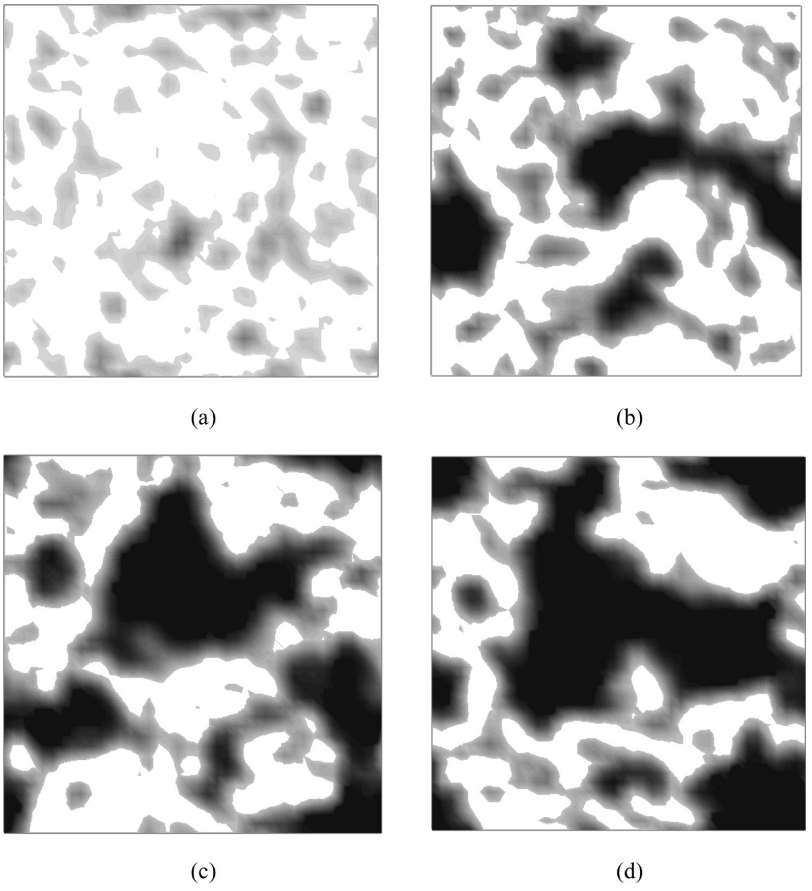


**Figure 4.** Contour plots of the density of the water beads as a 2D cross-section of the hydrated morphologies with EW = 640 and MW = 92 232 g/mol at water contents of (a) $\lambda = 6$, (b) $\lambda = 12$, (c) $\lambda = 18$, and (d) $\lambda = 24$ $H_2O/SO_3H$.

parameters by using the Blends module in Materials Studio, and the computed repulsion parameters are listed in Table 2. A simulation box size of $40 \times 40 \times 40$ was selected for our DPD simulations to include 192 000 DPD particles according to a density of $\rho = 3$. Following the method of Groot and Rabone, the interaction radius $r_c$ was determined to be about 8.14 Å, and the simulated time step was around 5.35 ps.[20]

**RDF Generation and Calculation of Bragg Spacing.** The distribution of beads about a lattice point $P$ is assumed to have a Gaussian form[46]

$$D_p(r) = \frac{N}{(2\pi\sigma^2)^{3/2}} \exp\left(-\frac{r^2}{2\sigma^2}\right) \tag{4}$$

in which $r$ is the distance from a reference lattice point, $N$ is the number density on the reference lattice point, and $\sigma$ is a standard distance. When the distribution of beads on a certain lattice point other than the reference lattice point is considered, the more useful asymmetric distribution function may be assumed and is given by

$$D(r) = \frac{N}{(2\pi)^{1/2}\sigma} \frac{r}{r_p} \left[\exp\left(-\frac{(r-r_p)^2}{2\sigma^2}\right) - \exp\left(-\frac{(r+r_p)^2}{2\sigma^2}\right)\right] \tag{5}$$

where $r_p$ is the distance from a lattice point $P$ to the reference lattice point $N$. By summing distributions from all of the lattice points around the reference lattice point, we obtain[20]

$$4\pi r^2 nG(r) = \frac{r}{(2\pi)^{1/2}} \sum_i \frac{N_i}{r_i\sigma_i} \left[\exp\left(-\frac{(r-r_i)^2}{2\sigma^2}\right) - \exp\left(-\frac{(r+r_i)^2}{2\sigma^2}\right)\right] \tag{6}$$

where $n$ is the average number density and $G(r)$ is the radial distribution function.

The scattering intensities $I(Q)$ can be related to the radial distribution function $G(r)$ by Fourier transformation for our finite-sized system[47,48] according to

$$I(Q,R) \equiv 4\pi\rho \int_0^R \mathrm{d}r\, r^2 \left[\frac{\sin(Qr)}{Qr}\right][G(r)-1] \tag{7}$$

where $Q$ is the magnitude of the scattering vector and $\rho$ is the average density over all space. The physical dimension or Bragg spacing ($d$) associated with the first peak at the maximum small-angle scattering vector $Q_m$ can then be evaluated from the Bragg relationship, $d = 2\pi/Q_m$.

(46) Yoon, B. J.; Jhon, M. S.; Eyring, H. Radial distribution function of liquid argon according to significant structure theory. *Proc. Nat. Acad. Sci. U.S.A.* **1981**, *78*, 6588−6591.

(47) Salacuse, J. J.; Denton, A. R.; Egelstaff, P. A. Finite-size effects in molecular dynamics simulations: static structure factor and compressibility 0.1. Theoretical method. *Phys. Rev. E* **1996**, *53*, 2382−2389.

(48) Salacuse, J. J.; Denton, A. R.; Egelstaff, P. A.; Tau, M.; Reatto, L. Finite-size effects in molecular dynamics simulations: static structure factor and compressibility 0.2. Application to a model krypton fluid. *Phys. Rev. E* **1996**, *53*, 2390−2401.

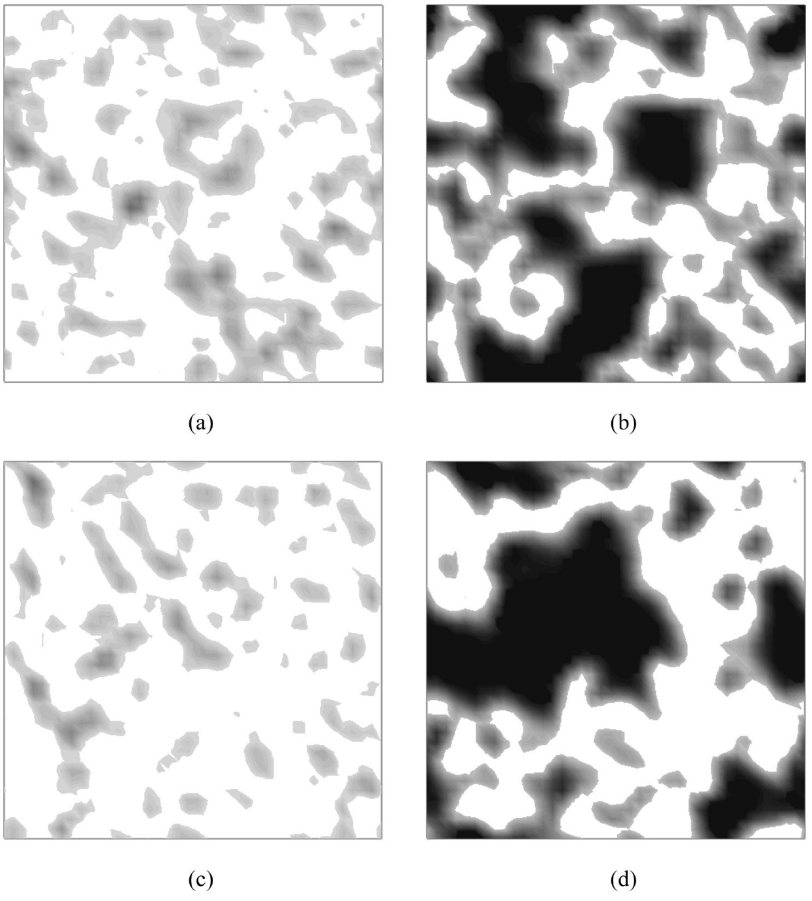


**Figure 5.** Contour plots of the density of the water beads in a 2D cross section for 3M PFSA ionomer with EW = 578 and MW = 90 168 g/mol at water contents of (a) $\lambda = 6$ and (b) $\lambda = 18$ $H_2O/SO_3H$; EW = 790 and MW = 88 536 g/mol at water contents of (c) $\lambda = 6$ and (d) $\lambda = 18$ $H_2O/SO_3H$.

## Results and Discussion

**Morphologies of Hydrated 3M PFSA Ionomers.** Various hydration levels, corresponding to $\lambda = 6$, 12, 18, and 24 $H_2O/SO_3H$, have been studied in the DPD simulations. These are equivalent to volumetric water contents of between 15.79 and 56.76% for an actual 3M membrane. Figure 2 shows the hydrated morphologies of the 3M PFSA ionomer with EW = 640 g/mol and MW = 46 116 g/mol in a simulation box with dimensions of approximately 32 nm cubed after about 5.35 ns of equilibration. Fluorocarbon beads of type A and B are red, hydrated ionic side-group beads of type C are green, and water beads of type W are blue. At a low hydration level, $\lambda = 6$ (Figure 2a), the water beads are distributed throughout the simulation box with only small regions of locally isolated water. With increasing hydration level, the formation of larger isolated aggregates of water beads occurs at $\lambda = 12$. However, only at high water contents, $\lambda = 18$ and 24, is the long-range connectivity of the water domains evident, which also gives rise to strong phase segregation with sharp interfaces between the fluorocarbon A/B beads and the water W beads. The general trend of enhanced water aggregation with increasing hydration level is consistent with the majority of simulation studies mentioned in the Introduction.

Figure 3 shows the corresponding contour plots of the density of W beads in a 2D cross section derived from the 3D cell contents in Figure 2. The 2D contour plots were created to align with the middle plane parallel to the first and second axes, and the level of darkness is proportional to the local water bead density. As shown in Figure 3a, water clusters are disconnected and show an irregular form at a low hydration level, $\lambda = 6$. With greater water content, as shown in Figure 3b for $\lambda = 12$, the water clusters increase in size and form a network with an irregular shape. At higher hydration levels of $\lambda = 18$ and 24 (Figure 3c,d, respectively), apparently continuous water-rich clusters are clearly discernible.

The contour plots of water density from a membrane with the same EW = 640 g/mol but a higher MW = 92 232 g/mol across the complete range of water contents are depicted in Figure 4. These show the same increase in cluster size and a sharpening of the water/fluorocarbon interface with increasing water content as those in Figure 3, except that each corresponding image in Figure 4 was produced from a PFSA ionomer with twice the MW. Hence, despite the similarities in the morphologies between the two different MWs, the water-rich domains in the ionomer with a higher MW became more elongated at a specific hydration level, as shown in Figure 4c,d as compared to Figure 3c,d, respectively. Because the main difference here is the longer poly(tetrafluoroethylene) (PTFE) backbone at higher MW, it can be suggested that the stretching of the backbone required to bring side-chain ionic groups into contact drives the formation of the elongated water domains, as found in our previous work on the SSC ionomer.[21] The calculation of the end-to-end distance distributions for the PFSA chains confirms that a significant proportion of those in Figure 4d are extended beyond the number expected for a random walk conformation. However, for the simulation boxes with the same density, the total number of ionic side-chain groups embedded with shorter backbones gain a higher degree of freedom. The morphology established here favors

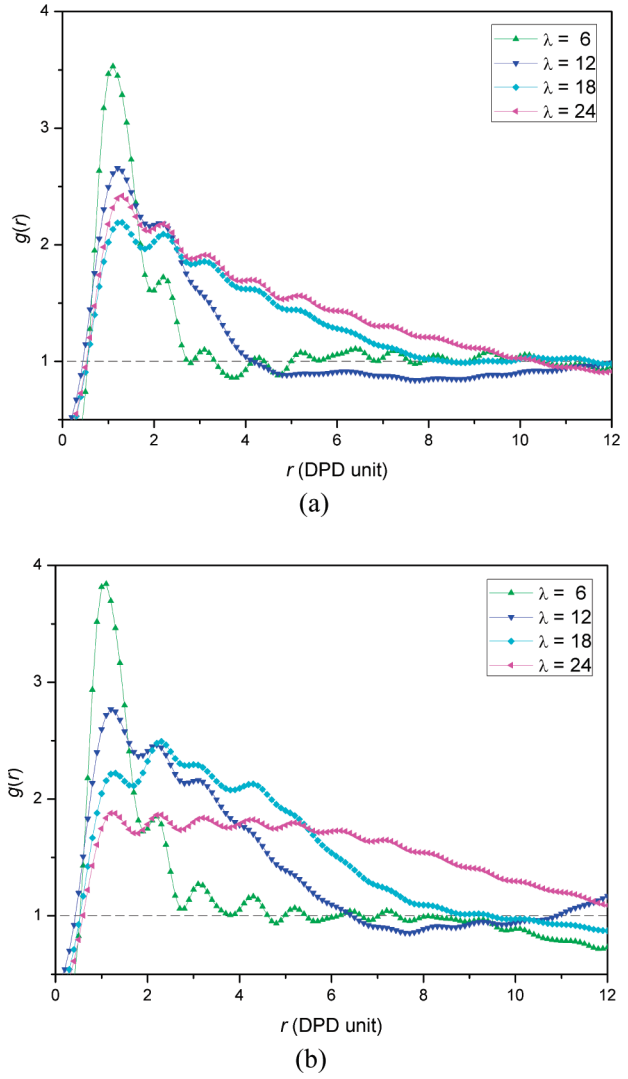


**Figure 6.** Radial distribution functions, $G(r)$, of water beads for the 3M PFSA membranes at various hydration levels: (a) EW = 578 and MW = 45 084 and (b) EW = 578 and MW = 90 168.

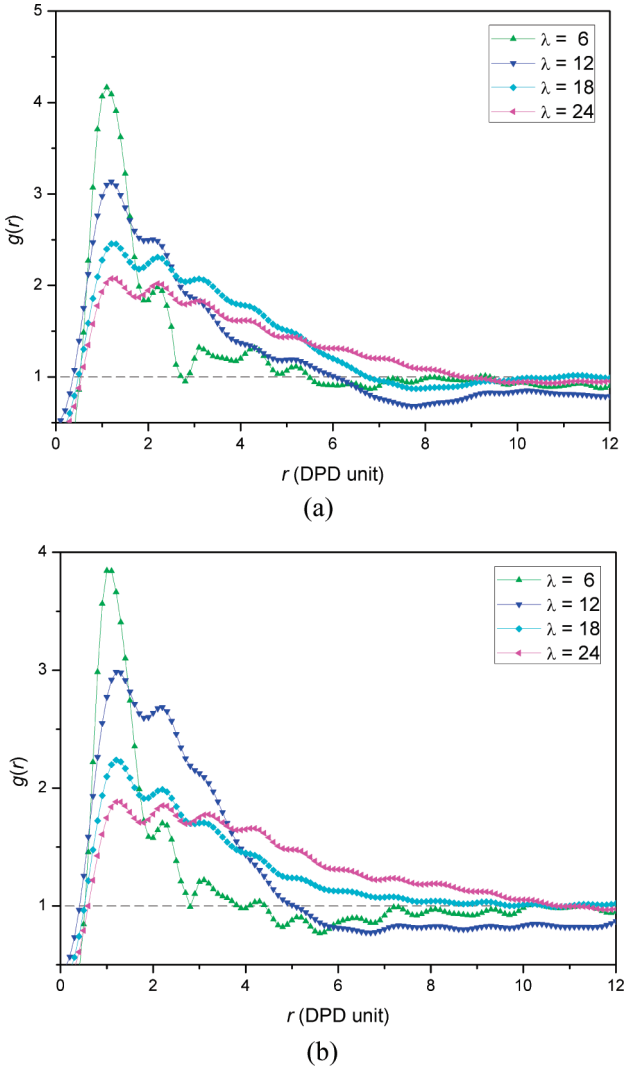


**Figure 7.** Radial distribution functions, $G(r)$, of water beads for the 3M PFSA membranes at various hydration levels: (a) EW = 790 and MW = 44 268 and (b) EW = 790 and MW = 88 536.

the proposition of neither a parallel water-channel model nor perfectly spherical clusters.[49,50]

Figure 5 shows water contour plots of water density from membranes with EW = 578 and MW = 90 168 g/mol (Figure 5a,b) together with EW = 790 and MW = 88 536 g/mol (Figure 5c,d) at hydration levels of $\lambda = 6$ and 18 $H_2O/SO_3H$ (Figure 5a,c, and Figure 5b,d, respectively). Both ionomer molecules have similar MWs but a different EWs. Indeed, much more significant changes in morphology caused by the increase in EW can be seen as compared to the effect of increasing MW shown between Figures 3 and 4. The main factor here is the higher percentage of the PTFE backbone at higher EW. This causes the extended spacing of water clusters, which is obvious and of no interest here. However, the longer backbone per ionic exchange group (i.e., higher EW) increases the repulsion between the hydrophobic and hydrophilic phases, which causes a stronger aggregation of water clusters. The effect can be clearly spotted by comparing parts a and c of Figure 5 and especially parts b and d of Figure 5. It can also be seen that at a higher hydration level of $\lambda = 18$ the number of smaller water clusters is reduced. This qualitatively illustrates why the water uptake is lower in membranes with a higher EW, corresponding to a lower ion-exchange capacity (IEC), because the aggregation of water into fewer but larger clusters is more difficult. From an experimental point of view, this effect is attributed to higher crystallinity at higher EW, which is consistent with our simulations even though we are not able to observe the fluorocarbon crystallites directly.

**Structural Analysis of Phase-Segregated Morphologies.** Figure 6 shows RDFs of water beads in 3M PFSA membranes with EW = 578 g/mol and MWs of 45 084 (Figure 6a) and 90 168 g/mol (Figure 6b). The high-frequency oscillations are attributed to the artificial smearing of discrete lattice densities. The plots show similar shapes and positions of peaks as the water content increases. This is probably due to the relatively rigid polymer framework. The first peak is steep at a hydration level of $\lambda = 6$, which implies a high density of water in small isolated clusters. As the hydration level increases, the second and higher peaks shift and merge, indicating the formation of more continuous water domains. The distance at which RDFs decay to the average density (i.e., $G(r) = 1$) increases accordingly, which characterizes the swelling of water domains with increasing water content.

(49) Schmidt-Rohr, K.; Chen, Q. Parallel cylindrical water nanochannels in Nafion fuel-cell membranes. *Nat. Mater.* **2008**, *7*, 75−83.

(50) Gierke, T. D.; Munn, G. E.; Wilson, F. C. The morphology in Nafion perfluorinated membrane products, as determined by wide- and small-angle X-ray studies. *J. Polym. Sci.* **1981**, *19*, 1687−1704.

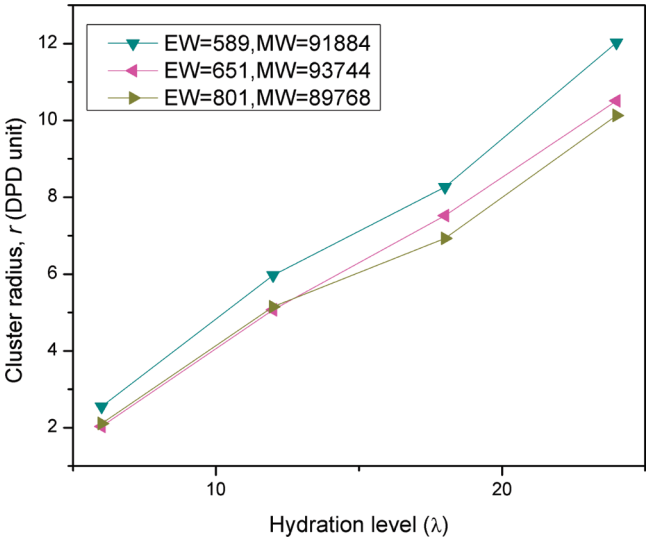


**Figure 8.** Average radius of water domains in 3M PFSA membranes with different EWs as a function of the hydration level.

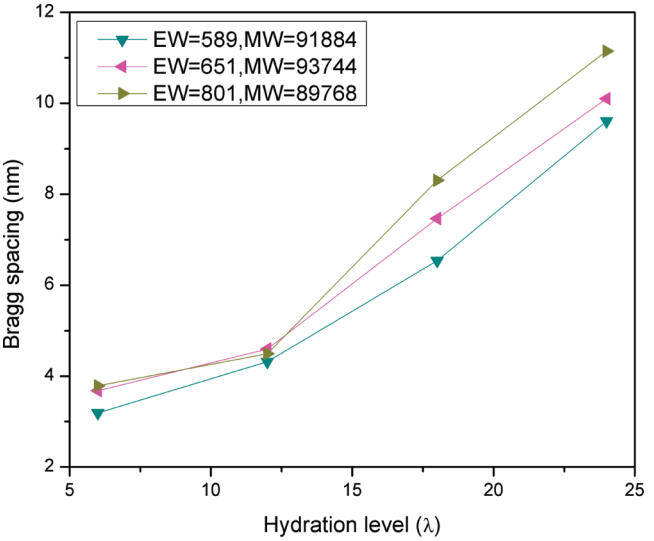


**Figure 9.** Bragg spacing, $d$, in 3M PFSA membranes with different EWs as a function of the hydration level.

This criterion will be further used to evaluate the average radius of water clusters quantitatively. By comparing Figure 6a,b, the most significant difference is that both the area under the RDF curves and mean density corresponding to intermediate hydration levels increase as the MW increases (Figure 6b). Therefore, it can be inferred that the spatial extent of water domains is generally increased as MW increases. This is mainly because of dominant repulsion between water and the longer PTFE backbone in the membrane with a higher MW.

Figure 7 shows RDFs of water beads in PFSA ionomers with the same EW = 790 g/mol and MWs of 44 268 (Figure 7a) and 88 536 g/mol (Figure 7b). The ionomer in Figure 7b has a similar MW to that in Figure 6b but a higher EW of 790 g/mol. The RDFs at hydration levels of $\lambda = 6$ and 12 show only minor differences between these two structures. However, at higher hydration levels of $\lambda = 18$ and 24, it can be seen that the RDFs have steeper curves. The steeper RDFs suggest a higher local water density, which corresponds to the stronger aggregation of water as described in the previous section. Furthermore, the fact that the peak following the first one falls to the average density much more quickly leads to the conclusion that there are smaller water domains in the ionomer with a higher EW in Figure 7b. The quantification of the average size of the water domains in ionomers with various EWs and similar MWs is shown in Figure 8. As expected from the above analysis of the RDFs, the sizes of the water domains are similar at a hydration level where $\lambda = 6$ and cross over at $\lambda = 12$ but then they follow a consistent trend in which the water domains increase in size as the EW decreases.

Finally, the structure factors were computed from the Fourier transformation of the radial distribution function. The first peak at scattering vector $Q_m$ associated with the ionomer peak was used to derive the Bragg spacing ($d$). Figure 9 shows the plots of $d$ as a function of the hydration level for the three membranes in Figure 8. The spacing of water domains shows the reverse trend as compared with the size of water domains when the EW of the membranes increases. This can be qualitatively assigned to the stronger repulsion on water clusters caused by the PTFE backbone and the stronger aggregation of water clusters. Although the spaces taken by the ionomers are similar because of the similar MWs, the longer PTFE backbone according to the larger EW will try to spread the water clusters out, hence resulting in the stronger aggregation of water domains.

## Conclusions

In this work, we have studied the hydrated morphologies of 3M PFSA membranes using DPD simulations. As the water content increases, the locally isolated water clusters at a low hydration level become a continuous water domain at a high hydration level. The MW has a strong influence on both the shape and size of the water clusters. The longer PTFE backbone, corresponding to a higher MW, drives the elongated form in water-rich ionic phase. The effect of the EW on the morphology has also been evaluated. A higher EW corresponding to a lower IEC favors the stronger aggregation of separated phases, which accordingly results in a lower water uptake. This effect may be attributed to higher crystallinity at a higher EW, although our simulations were not able to show the fluorocarbon crystallites directly.

**Acknowledgment.** This work was supported by the DOE under contract number DE-FG36-07G017006. DOE support does not constitute an endorsement by the DOE of the views expressed in this work.